EFFECTIVE STRESS METHOD IN ONE-DIMENSIONAL SOIL RESPONSE ANALYSIS

Kenji Ishihara(1) and Ikuo Towhata(2)

SUMMARY

A method of dynamic effective stress analysis is developed on the basis of an effective stress path model embodied into the theory of wave propagation through porous media. In this method the shear modulus used in the horizontal ground response analysis is evaluated continuosly as the vertical effective stress at each depth of the deposit changes with time. The above analytical procedures were applied to a liquefaction study of a site near the city of Niigata where liquefaction-induced ground failure had occurred during the 1964 earthquake.

STRESS PATH MODEL

(1) Description of the model

The prediction of pore water pressure changes during seismic loading is made by means of a modified version of the stress path model proposed previously by Ishihara et al. (1975). In its original form the pore water pressure was assumed to build up only during the virgin loading phase which occurred whenever the loading path cuts across the current yield surface established by previous levels of loading. Unloading and reloading were assumed to induce purely elastic deformations and cause no changes in pore water pressure or effective stresses. This assumption that no pore water pressure change is associated with unloading and reloading phases is not supported by experimental data, especially where the application of shear stress involves a number of more or less constant-amplitude cyclic loading. In order to improve this inadequacy of the model, a modification is made by incorporating the plastic deformation during unloading and reloading. This secondary plastic deformation accompanies the build-up of pore water pressures. The procedure for predicting the increases in pore water pressures in saturated sand subjected to a sequence of irregular loading under undrained conditions is illustrated in Fig.1. Fig.1b shows the effective stress path drawn in the σ_v'-τ stress space, where σ_v' and τ denote the vertical effective stress and the shear stress in the simple shear condition, respectively. The loading from the initially consolidated state 1 to a new stress state 2 causes a plastic deformation and generates an increase in the pore water pressure. During this virgin loading the yield surface is shifted upwards to a new yield surface, represented by a straight line connecting the origin and point 2 in Fig.1b. The curve 1-2 is assumed to be a parabola given by,

$$\sigma_v' = m - \frac{B_p'}{m}\tau^2 \quad \cdots\cdots\cdots\cdots\cdots\cdots\cdots\cdots\cdots\cdots\cdots\cdots\cdots\cdots\cdots\cdots\cdots\cdots \quad (1)$$

where B_p' is a soil constant representing the characteristics of pore water pressure build-up, and m is a parameter for locating a current parabolic stress path at each time step of computation. Unloading from point 2 to 3

(1) Professor of Civil Engineering, University of Tokyo
(2) Graduate Student, University of Tokyo

and reloading back to point 4 takes place entirely inside the current yield surface. The deformation that occurs during this stress change is considered secondary plastic, and pore water pressure is assumed to build up according to an empirical formula given by

$$\left.\begin{aligned} &\Delta\sigma_v' = -B_u' \left(\frac{\tau}{\sigma_{v0}'} - \frac{\tau_m}{\sigma_{v0}'} \right)\left(\frac{\sigma_v'}{\sigma_{v0}'} - \kappa \right)\Delta\tau \qquad \text{for} \quad \sigma_v' \geq \kappa\sigma_{v0}' \\ &\text{or} \quad \Delta\sigma_v' = 0 \qquad\qquad\qquad\qquad\qquad\qquad \text{for} \quad \sigma_v' < \kappa\sigma_{v0}' \end{aligned}\right\} \quad \cdots (2)$$

where σ_{v0}' is the vertical consolidation pressure, $\Delta\tau$ is the change in shear stress and τ_m is the maximum shear stress that has been applied to the soil in the most recent cycle as illustrated in Fig.2. The value, B_u', is a soil constant representing the pore water pressure build-up characteristics during the unloading and reloading phases. The value, κ, was introduced to account for the fact that the pore water pressure ceases to build-up when the remaining vertical effective stress decreases to a certain value. In the present study it is assumed that $\kappa = 0.1$. A continued loading from point 4 to 5 takes a parabolic stress path and cuts across the yield surface and causes plastic deformation which in turn brings about an increase in pore water pressure. Unloading from point 5 to 6 is also secondary plastic. Yielding in the stress space above the σ_v'-axis is assumed to occur independent of the yielding in the stress space below and vice versa; therefore, loading from point 6 to 7 causes plastic deformation and increases pore water pressures, again following a parabolic curve. The stress path from point 7 to 18 follows the above pattern. Point 18 lies on what is termed the phase transformation line, and it is assumed that unloading from any stress point on the outside of the phase transformation line reduces the effective stress to zero and causes liquefaction.

The values of the phase transformation angle, θ_s', in isotropically consolidated soils, i.e., in $K_0 = 1.0$ condition are determined by an empirical relation, $\tan\theta_s' = 0.87 \tan\phi$, where ϕ is the angle of internal friction of the soils. The constants, B_p', and, B_u', are determined from cyclic triaxial shear test results expressed in terms of the cyclic stress ratio causing initial liquefaction in 5 and 20 cycles, R_5 and R_{20}, respectively. To facilitate the determination of the values of B_p' and B_u', a chart is provided as shown in Fig.3 for the case of $\tan\theta_s' = 0.5$ or $\theta_s' = 26.6°$. In this figure, the values of B_p' and B_u' for the particular value of $\theta_s' = 26.6°$ are indicated by the notations $\bar{B}_p$ and $\bar{B}_u$. In using the chart in Fig.3, the known values of R_5 and R_{20} are transformed into $\bar{R}_5$ and $\bar{R}_{20}$ through the formulae

$$\bar{R}_5 = \frac{R_5}{2\tan\theta_s'}, \quad \bar{R}_{20} = \frac{R_{20}}{2\tan\theta_s'} \qquad \cdots\cdots\cdots\cdots\cdots\cdots (3)$$

With $\bar{R}_5$ and $\bar{R}_{20}$ known, one can select corresponding solid and dashed curves shown in Fig.3. Then, it becomes possible to locate a point of intersection of these two curves. The ordinate and the abscissa of this intersection give the values of $\bar{B}_p$ and $\bar{B}_u$ to be used in the pore water pressure model. For the general case of the phase transformation angle different from $\theta_s' = 26.6°$, the following transformation is made to determine the values of B_p' and B_u',

$$B_p' = \frac{\bar{B}_p}{(2\tan\theta_s')^2}, \quad B_u' = \frac{\bar{B}_u}{(2\tan\theta_s')^2} \qquad \cdots\cdots\cdots\cdots (4)$$

(2) Effects of K_0-conditions

The above pore water pressure parameters are determined from the results of the cyclic triaxial or simple shear tests conducted for isotropically consolidated samples. The constants, θ_s', B_p' and B_u' for the conditions of K_0-values less than unity are estimated from the values obtained for $K_0 = 1.0$. The horizontal shear stress in a condition of $K_0 = 1.0$ is denoted by τ' and the shear stress under the condition of $K_0 \neq 1.0$ by τ. Then, the stress ratios under isotropically consolidated state and anisotropically consolidated state are correlated with each other as follows,

$$\frac{\tau}{\sigma_v'} = \frac{1 + 2K_0}{3} \frac{\tau'}{\sigma_v'} \qquad \cdots\cdots\cdots\cdots\cdots\cdots\cdots\cdots (5)$$

Then, using Eq.(5) with reference to Eqs.(1) and (2), the phase transformation angle, θ_s', values of B_p' and B_u' for the general K_0-conditions can be obtained as follows,

$$\left.\begin{aligned} \tan\theta_s &= \frac{1 + 2K_0}{3} \tan\theta_s' \\ B_p &= \left(\frac{3}{1 + 2K_0}\right)^2 B_p' = \left(\frac{3}{2(1 + 2K_0)\tan\theta_s'}\right)^2 \bar{B}_p \\ B_u &= \left(\frac{3}{1 + 2K_0}\right)^2 B_u' = \left(\frac{3}{2(1 + 2K_0)\tan\theta_s'}\right)^2 \bar{B}_u \end{aligned}\right\} \cdots (6)$$

in which θ_s, B_p and B_u denote the value of θ_s', B_p' and B_u' in the general case where the K_0-value and the phase transformation angle can take any value.

STRESS-STRAIN MODEL

In order to compute the dynamic response of horizontally layered deposits of soil subjected to the upward propagating shear waves, a nonlinear relationship describing the histeresis of stress and strain must be established. For the initial virgin loading, the relationship between the shear stress, τ, and shear strain, γ, is given by

$$\tau = \frac{G_t \gamma}{1 + \dfrac{\gamma}{\gamma_r}}, \quad \gamma_r = \frac{\tau_f}{G_t} \qquad \cdots\cdots\cdots\cdots\cdots\cdots (7)$$

where G_t is the initial tangent shear modulus, τ_f is the shear strength of soils and γ_r is reference strain. The value of G_t is calculated by the formula (Iwasaki-Tatsuoka, 1977),

$$G_t = 14{,}000 \frac{(2.17 - e)^2}{1 + e} \left(\frac{1 + 2K_0}{3} \sigma_v'\right)^{0.4} \quad (kN/m^2) \cdots (8)$$

where e is the void ratio. The shear strength of soils, τ_f, is given by

$$\tau_f = \sigma_v' \tan\phi' + c \qquad \cdots\cdots\cdots\cdots\cdots\cdots\cdots\cdots (9)$$

in which ϕ' is the angle of internal friction and c is the cohesion.

For the subsequent unloading and reloading cycles the Masing law (Finn et al., 1977) is applied to construct the hysteristic loops based on the skeleton curve given by Eq.(7).

EQUATION OF MOTION FOR DYNAMIC RESPONSE ANALYSIS

The dynamic response of the horizontally layered deposits of soils is determined by solving the following equation of motion in combination with the stress-strain relationship established in the preceding section.

$$\frac{\gamma_t}{g}\frac{\partial^2 u_x}{\partial t^2} = \frac{\partial \tau}{\partial z} \qquad \cdots\cdots (10)$$

where u_x denotes the horizontal displacement, τ is the shear stress, γ_t denotes the unit weight of soil, and g is the acceleration of gravity. The z-coordinate is taken downward from the ground surface as indicated in Fig. 4.

EQUATIONS OF MOTION AND SEEPAGE IN THE VERTICAL DIRECTION

Basic equations of motion are derived from the general equations in the theory of water-saturated porous media. Denoting the vertical velocity of the soil by W and the vertical velocity of water flow relative to the soil movement by Q, the equations of motion are written as (Ishihara-Towhata, 1980)

$$\left.\begin{aligned} &\frac{\gamma_t}{g}\frac{\partial W}{\partial t} + \frac{\gamma_w}{g}\frac{\partial Q}{\partial t} = \frac{\partial \sigma}{\partial z} - \gamma_t \\ &\frac{n\gamma_w}{g}\frac{\partial W}{\partial t} + \frac{\gamma_w}{g}\frac{\partial Q}{\partial t} + \frac{bQ}{n} - n\frac{\partial u}{\partial z} + n\gamma_w = 0 \end{aligned}\right\} \qquad \cdots\cdots (11)$$

where σ and u denote the vertical total stress and the pore water pressure, respectively, n is the porosity of soil, and γ_w is the unit weight of water. The constant, b, in Eq.(11) is given by $b = n^2\gamma_w/k$, where k is the permeability.

If the compressibilities of solid and water constituting the two-phase medium are neglected, the volumetric strain expressed in terms of W and Q must satisfy the volumetric compatibility equation,

$$\frac{\partial W}{\partial z} + \frac{\partial Q}{\partial z} = 0 \qquad \cdots\cdots (12)$$

The detailed procedure for deriving Eq.(12) is described elsewhere (Ishihara-Towhata, 1980).

The pore water pressure generated at any depth in the soil deposit can be assessed by the use of the stress path model described above in the preceding section. However, if the soil deposit can drain during shakeing, dissipation of pore water will take place simultaneously. Thus, the rate of increase of pore water pressure will be less than that for completely undrained case. The distribution of pore water pressure is governed by the equation,

$$\frac{\partial W}{\partial z} = m_v \left(\frac{\partial \sigma}{\partial t} - \frac{\partial u}{\partial t} + \frac{\partial u_g}{\partial t} \right) \quad \cdots\cdots\cdots\cdots\cdots\cdots\cdots\cdots \quad (13)$$

where m_v is the coefficient of volume compressibility, and u_g denotes the internally generated pore water pressure evaluated with the use of the stress path model.

NUMERICAL INTEGRATIONS

For the horizontal dynamic response analysis, the horizontal soil deposit is divided into layers. These layers are converted to a lumped mass system by concentrating one-half of the mass of each layer at the layer boundaries as shown in Fig.4. Input motions are applied to the mass nearest to the base through a viscous damping which is incorporated in order ro take into account the effect of energy loss due to dispersion of wave energy. The masses are connected by nonlinear springs with the stress-strain properties described by stress-strain model. The numerical integration with time is made stepwise for the set of simultaneous differential equations established for the lumped mass system using the Newmark's β-method with $\beta = 1/4$. At each time step of integration, the stress-strain relationship is updated through Eq.(8) in order to take into account the changes in the vertical effective stress which is calculated in the pore water pressure analysis described below.

For the dissipation of pore water pressure in the vertical direction, Eqs.(11), (12) and (13) were numerically integrated stepwise with respect to time using the method of weighted residuals (Zienkiewicz, 1977). The soil deposit is divided into layered elements in the same manner as adopted in the horizontal response analysis (Fig.4). The upward migration of the water table near the surface of the soil deposit as the dissipation of pore water pressure proceeds is taken into account in the effective stress analysis. A flow chart indicating the interplay between the models and the sets of equations is presented in Fig.5.

ANALYSIS OF A NIIGATA SITE DURING THE 1964 EARTHQUAKE

Detailed soil investigations were made recently using a large diameter sampling technique, in the flood plain of the lower reaches of the Agano river located east of the city of Niigata. Signs of liquefaction such as surface crackings and sand volcanos were observed at this site at the time of the 1964 earthquake. Undisturbed sand samples were obtained to a depth of 7 m and tested in the laboratory using a cyclic triaxial test apparatus. The soil profile established in this investigation and the properties within each divided layer is shown in Fig.6. The coefficient of volume compressibility, m_v, was estimated using the formula proposed by Finn et al. (1977). The permeability coefficient, k, was estimated on the basis of the Hazen's empirical formula (Terzaghi-Peck, 1967). The blow count values obtained in a nearby boring were used to estimate the soil properties in the deposit more than 7 m. The input base was assumed to lie at a depth of 25 m. The shear wave velocity and unit weight of the base material were estimated to be V_R = 600 m/sec. and γ_R = 20 kN/m^3, respectively.

At the time of the 1964 earthquake, acceleration records were obtained in the basement of the prefectural government office building standing on the hard deposit in the city of Akita located approximately 180 km distant from the epicenter. The fact that the Agano river site lies approximately

45 km from the epicenter requires rescaling of the predominant period of the original acceleration record in the N-S component from 0.675 sec. to a more appropriate predominant period of 0.4 sec. The amplitude of the acceleration record was also reduced to a maximum acceleration of 50 gal and used as an incident input motion at the base of the deposit. The acceleration time history is shown in Fig.7.

The computed acceleration time histories at several depths of the deposit are shown in Fig.7, where it is noted that around 4.5 seconds after the initiation of the shaking liquefaction develops in the soft layers near the surface. The distribution of the computed maximum acceleration is shown in Fig.8. The maximum acceleration on the ground is 0.165 g and this is in agreement with the acceleration of 0.162 g recorded during the 1964 earthquake. The distributions of the pore water pressure versus depth at several instances of time during dynamic loading are shown in Fig.9. It is seen in these figures that the pore water pressure builds up gradually as the shaking proceeds and at 4.5 seconds after the initiation of the shaking the loose layer near the surface is brought into the state of liquefaction.

CONCLUSIONS

With the use of the dynamic effective stress method of one-dimensional soil response analysis, a liquefaction analysis was made for a loose sand deposit at the Agano river site in Niigata, Japan, where signs of liquefaction were observed in the 1964 earthquake and also where detailed soil investigation were performed after the quake. The result of analysis showed that when the first peak acceleration in time history occurs the effective stress becomes zero inducing liquefaction throughout the loose deposit to a depth of 8.0 m. The maximum horizontal acceleration becomes 0.165 g on the ground surface which is in agreement with the acceleration recorded at the time of the 1964 earthquake.

ACKNOWLEDGEMENTS

The original draft of this paper was kindly edited by Dr. K. Mori.

REFERENCE

Finn, W. D. L., Lee, K. W., and Martin, G. R. (1977), "An Effective Stress Model for Liquefaction," Proc. ASCE, Vol.103, GT. 6, pp.517-533.

Ishihara, K., Tatsuoka, F., and Yasuda, S. (1975), "Undrained Deformation and Liquefaction of Sand under Cyclic Stresses," Soils and Foundations, Vol.15, No.1, pp.29-44.

Ishihara, K. and Towhata, I. (1980), "Response Analysis of Level Ground Based on Effective Stress Method," (in preparation).

Iwasaki, T., and Tatsuoka, F. (1977), "Effects of Grain Size and Grading on Dynamic Shear Moduli of Sands," Soils and Foundations, Vol.17, No.3, pp.19-35.

Terzaghi, K., and Peck, R. B. (1967), "Soil Mechanics in Engineering Practice," Fohn Wiley & Sons, INC. p.50.

Zienkiewicz, O. C. (1977), The Finite Element Method, 3rd Edition, MacGraw-Hill, p.49.

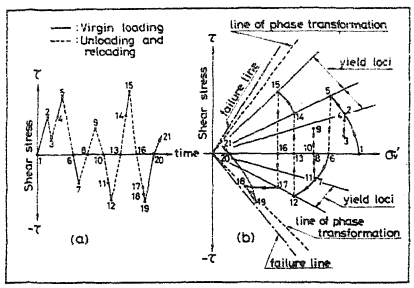

Fig.1 Original stress path model

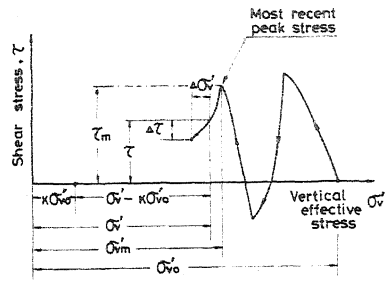

Fig.2 Stress path for unloading phase

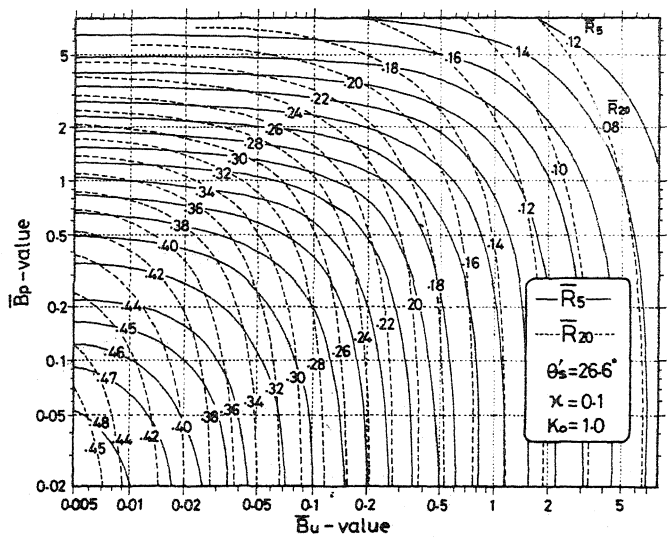

Fig.3 A chart for the constants, $\bar{B}_p$ and $\bar{B}_u$

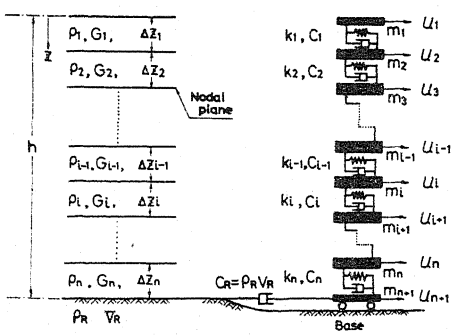

Fig.4 Lumped mass system for response analysis

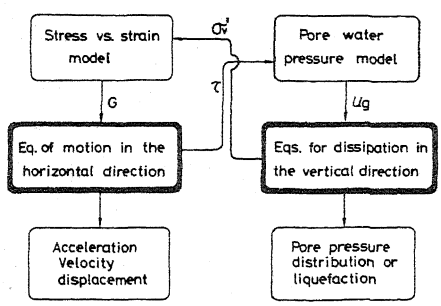

Fig.5 Flow chart of the numerical scheme

Z (m)	Layer div.	Porosity n_e	Unit weight γ_t	G_{ma}	ϕ^*	Cohesion	Gt**	Static strength τ_f
	1	0.48		8.41	35	10	28900	13.5
	2	"		13.38	38	0	40800	10.8
	3	"		19.85	"	"	40800	16.1
5	4	"		28.47	"	"	72000	23.1
	5	"		38.27	"	"	72000	31.0
	6	"		48.25	"	"	95200	39.9
	7	"	"	61.01	"	"	131000	48.7
	8	0.40	19	75.71	40	"	348000	63.5
10	9	0.38	19.5	93.84	43	"	348000	87.5
	10	"	"	111.5	"	"	450000	104.0
15	11	"	"	129.2	"	"	504000	120.5
	12	Agano river site (Niigata)		148.8	"	"	506000	138.7
	13			168.3	"	"	450000	157.0
20	14			186.9	"	"	450000	174.3
	15	"	"	205.6	"	"	450000	191.7
25	16	"	"	219.5	"	"	487000	204.7

* Angle of internal friction
** Shear modulus at small strains

Z (m)	Layer div.	θ_s*	Cyclic strength Rs	Cyclic strength R_{20}	Bp	Bu	m_v** (m^2/kN)	Ko-value	Permeability, k (m/sec)
	1							0.8	10^{-2}
	2	35	0.190	0.160	9.4	0.23	3.08×10^{-4}	0.5	10^{-4}
	3	"	0.190	0.165	"	"	2.65 "	"	"
	4	"	0.225	0.178	6.1	0.37	2.31 "	"	"
5	5	"	0.210	0.190	8.0	0.11	2.07 "	"	"
	6	"	0.210	0.180	7.8	0.22	1.84 "	"	"
	7	"	0.200	0.170	8.5	0.23	1.73 "	"	"
	8	36	0.620	0.410	0.015	0.059	1.49 "	0.7	"
10	9	39	0.580	0.390	0.01	0.086	1.33 "	0.8	"
	10	"	0.580	0.370	0.018	0.13	1.25 "	"	"
15	11	"	0.600	0.400	0.01	0.081	1.18 "	"	"
	12	"	0.670	0.440	"	0.051	1.12 "	Agano river site (Niigata) Base rock: γ_B =20kN/m³ V_B=600m/sec	
	13	"	0.640	0.430	"	0.066	1.07 "		
20	14	"	0.540	0.360	0.061	0.13	1.02 "		
	15	"	0.520	0.350	0.14	"	9.88×10^{-5} "	"	"
25	16	"	0.570	0.380	0.03	0.11	9.64 "	"	"

* Phase transformation angle in K_o=1.0 conditions
** Coefficient of volume compressibility

Fig.6 Soil constants used for the analysis

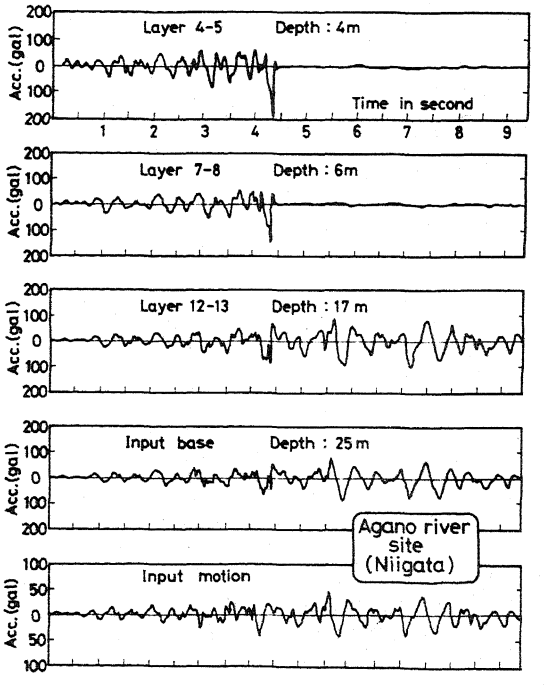

Fig.7 Computed acceleration at several depths

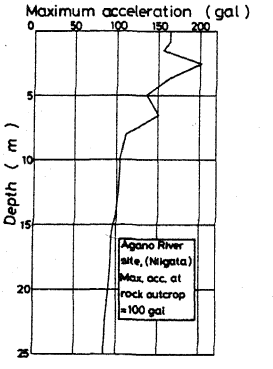

Fig.8 Distribution of the computed maximum accelerations

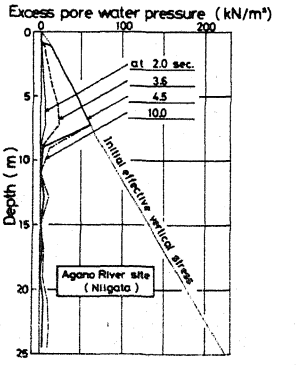

Fig.9 Pore water pressure at several instances of time